SMM 4402
24 July 2003 Disk used
ARTICLE IN PRESS
No. of Pages 5, DTD = 4.3.1

Available online at www.sciencedirect.com
SCIENCE DIRECT®

PERGAMON

Scripta Materialia xxx (2003) xxx–xxx

Scripta MATERIALIA
www.actamat-journals.com

Evolution of crystal orientation distribution coefficients during plastic deformation

D.S. Li [a], H. Garmestani [a,*], Scott Schoenfeld [b]

[a] *School of Materials Science and Engineering, Georgia Institute of Technology, 771 Ferst Drive, N.W. Rm 175, Lov., Atlanta, GA 30332, USA*
[b] *Aberdeen Proving Ground, Maryland, MD 21005-5066, USA*

Received 15 April 2003; received in revised form 16 July 2003; accepted 17 July 2003

1. Introduction

Properties of polycrystalline materials are dependent on the orientation distribution of crystal grains, also called texture. It is usually represented as a Fourier series of generalized spherical harmonics weighted by appropriate texture coefficients [1]. Microstructures can be represented as points in a multidimensional space (microstructure hull) with coordinates as texture coefficients [2]. Microstructure sensitive design as proposed earlier by Adams et al. [2] introduces a new methodology to establish processing paths in the microstructure hull. Optimization of texture in microstructures requires correct representation of these processing paths. Clement and Coulomb [3,4] proposed a principle of conversation of quantity of matter referred to a given crystal orientation during processing of microstructures in the orientation space. This can be used to produce processing paths in the microstructure hull for a certain process from the initial texture. Based on Clement's formalism and the continuity equation, Bunge and Esling [5] studied the flow field of single crystals of face centered cubic (fcc) metals according to $(1\,1\,1)\langle 1\,1\,0\rangle$ slip.

The present study proposes an alternate approach using a polycrystalline materials description rather than single crystal orientation description. This approach establishes a linear relationship between the rate of change of the texture coefficients and the initial texture. To examine the accuracy and range of applicability of this linear approach, a modified Taylor's model proposed by Kalidindi etc. [6,7] was used for comparison. In Taylor's model, it is assumed that all the individual grains in the polycrystalline material undergo the same deformation gradient as the macroscopic one. This simplification satisfies the local compatibility, but often violates equilibrium. Although Taylor's model ignores many of the complexities of material's deformation, it provides a fairly accurate approximate solution for the texture evolution of single phase, highly symmetric lattice structures, such as fcc polycrystals, during large plastic deformation [7].

2. Rate of change of texture coefficient during plastic deformation

At any point during deformation, texture can be represented by a set of Fourier coefficients $F_l^{mn}(\eta)$,

* Corresponding author. Tel.: +1-404-385-4495; fax: +1-404-894-9140/678-623-3920.
E-mail address: hamid.garmestani@mse.gatech.edu (H. Garmestani).

1359-6462/$ - see front matter © 2003 Published by Elsevier Ltd. on behalf of Acta Materialia Inc.
doi:10.1016/S1359-6462(03)00443-3

where η is an appropriate metric of the processing step [5]. For example, in a drawing step, η represents the drawing strain. The orientation distribution function at a specified processing step η, $f(g,\eta)$ of the polycrystalline materials can be represented as a series of generalized spherical harmonic functions:

$$f(g,\eta) = \sum_{l=0}^{\infty} \sum_{m=0}^{M(l)} \sum_{n=0}^{N(l)} F_l^{mn}(\eta) \ddot{T}_l^{mn}(g) \tag{1}$$

$\ddot{T}_l^{mn}(g)$ are symmetric generalized spherical harmonics for the corresponding sample and crystal symmetry. The continuity relations obtained from the principle of conservation in the orientation space can be expanded in a series of spherical harmonics [5]:

$$\sum_{\lambda\sigma\rho} F_\lambda^{\sigma\rho}(\eta)\, \mathrm{div}(\ddot{T}_\lambda^{\sigma\rho}(g)R(g)) + \sum_{lmn} \frac{\mathrm{d}F_l^{mn}(\eta)}{\mathrm{d}\eta} \ddot{T}_l^{mn}(g) = 0 \tag{2}$$

Here $R(g)$ defines the rotation field. The first term describes the increase of the quantity of matter in the orientation space moving out of a infinitesimal volume in the orientation space dg. The second term describes the decrease of quantity of matter per unit time. The divergence function in the first term can be expanded further into a series of generalized spherical harmonics:

$$\mathrm{div}(\ddot{T}_\lambda^{\sigma\rho}(g)R(g)) = \sum_{lmn} A_{l\lambda}^{mn\sigma\rho} \ddot{T}_l^{mn}(g) \tag{3}$$

Substituting this expansion into Eq. (2), we find the linear relationship between the texture coefficients and their rate of change:

$$\frac{\mathrm{d}F_l^{mn}(\eta)}{\mathrm{d}\eta} = \sum_{\lambda\sigma\rho} A_{l\lambda}^{mn\sigma\rho} F_\lambda^{\sigma\rho}(\eta) \tag{4}$$

This linear relationship was used by Bunge to predict the texture evolution for single crystal orientations. In this study, we will use this relationship to simulate the texture evolution of fcc materials with random texture and examine its accuracy. If the number of texture coefficients F_l^{mn} is limited to N, then texture data for $N+1$ different strains will be needed to obtain a solution for the texture evolution coefficient $A_{\lambda l}^{\sigma\rho mn}$. Further the sixth rank tensor coefficients are represented by an $N \times N$ matrix as outlined later in the paper.

3. Results

Taylor's model is used in the present study to provide the corresponding F_l^{mn} and their change for different strains, η. Using these coefficients in Eq. (4), we obtain the solution for $A_{\lambda l}^{\sigma\rho mn}$. To check the validity of this approach, we use the resultant $A_{\lambda l}^{\sigma\rho mn}$ to predict texture at other strains and compare the results with that predicted by Taylor's model. The initial texture in this study is assumed to be an aggregate of 400 crystals evenly distributed in the orientation space. The corresponding (1 0 0), (1 1 0) and (1 1 1) pole figures of this data set are illustrated in Fig. 1. The maximum intensity is very small, less than 1.5 times random.

For the present study, face centered cubic crystal system is assumed along with orthotropic sample symmetry. The texture coefficients F_l^{mn} with $l > 4$ do not affect elastic properties for cubic polycrystalline materials [8] and as a result a

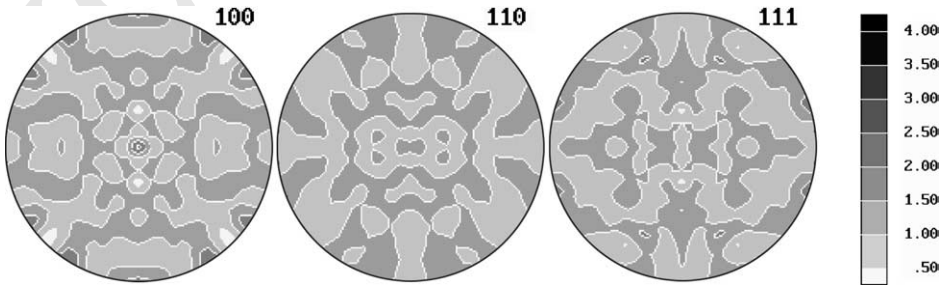

Fig. 1. (1 0 0), (0 1 0) and (0 0 1) pole figures of initial simulated random texture by 400 crystals.

minimum value of 4 is chosen for the order of rank l of the Fourier series F_l^{mn} in Eq. (1). For this case there are four nonzero F_l^{mn} coefficients in which F_0^{11} is a constant (always 1.0). This reduces the number of nonzero texture coefficients to only three terms: F_4^{11}, F_4^{12} and F_4^{13}. That is to say, $N = 3$.

From Eq. (4), we have:

$$\frac{\mathrm{d}F_4^{11}(\eta)}{\mathrm{d}\eta} = A_{44}^{1111}F_4^{11} + A_{44}^{1112}F_4^{12} + A_{44}^{1113}F_4^{13} + \cdots = A_{44}^{1111}F_4^{11} + A_{44}^{1112}F_4^{12} + A_{44}^{1113}F_4^{13} \tag{5.1}$$

$$\frac{\mathrm{d}F_4^{12}(\eta)}{\mathrm{d}\eta} = A_{44}^{1211}F_4^{11} + A_{44}^{1212}F_4^{12} + A_{44}^{1213}F_4^{13} \tag{5.2}$$

$$\frac{\mathrm{d}F_4^{11}(\eta)}{\mathrm{d}\eta} = A_{44}^{1311}F_4^{11} + A_{44}^{1312}F_4^{12} + A_{44}^{1313}F_4^{13} \tag{5.3}$$

or,

$$\begin{bmatrix} \mathrm{d}F_4^{11}/\mathrm{d}\eta \\ \mathrm{d}F_4^{12}/\mathrm{d}\eta \\ \mathrm{d}F_4^{13}/\mathrm{d}\eta \end{bmatrix} = \begin{bmatrix} A_{44}^{1111} & A_{44}^{1112} & A_{44}^{1113} \\ A_{44}^{1211} & A_{44}^{1212} & A_{44}^{1213} \\ A_{44}^{1311} & A_{44}^{1312} & A_{44}^{1313} \end{bmatrix} \begin{bmatrix} F_4^{11} \\ F_4^{12} \\ F_4^{13} \end{bmatrix} \tag{6}$$

Here $A_{l\lambda}^{mn\sigma\rho}$ are components of a sixth order tensor. These cumbersome indices emphasize the character of the tensors. To simplify the indices, Eq. (6) is rewritten in the following contracted form:

$$\begin{bmatrix} \mathrm{d}F_1/\mathrm{d}\eta \\ \mathrm{d}F_2/\mathrm{d}\eta \\ \mathrm{d}F_3/\mathrm{d}\eta \end{bmatrix} = \begin{bmatrix} A_{11} & A_{12} & A_{13} \\ A_{21} & A_{22} & A_{23} \\ A_{31} & A_{32} & A_{33} \end{bmatrix} \begin{bmatrix} F_1 \\ F_2 \\ F_3 \end{bmatrix} \tag{7}$$

In this way we simplify the solution of a sixth order tensor of texture evolution coefficient to a second order matrix operation by reducing the number of texture coefficients to only the ones which are of interest.

For the analysis, first the texture evolution coefficients $A_{\lambda l}^{\sigma\rho mn}$ are calculated from $N+1$ texture data obtained by Taylor's model at different strains. Then these coefficients are used to simulate the rate of change of the texture coefficients at other points in the deformation path. These rates are compared with the predictions from Taylor's model. In the first set, a strain step of 1% is used. The F_l^{mn} s at strains of 30%, 31%, 32% and 33% are calculated from Taylor's model. Here these strains are called the initial strain set. From the texture coefficient rates $\mathrm{d}F_l^{mn}/\mathrm{d}\eta$ and the texture coefficients F_l^{mn} at different strains, $A_{\lambda l}^{\sigma\rho mn}$ s are calculated. Using the sixth rank tensor evolution parameters $A_{\lambda l}^{\sigma\rho mn}$, the rates of change of texture coefficients, $\mathrm{d}F_l^{mn}/\mathrm{d}\eta$ at strains from 20% to 50%, were computed. This process was repeated for a strain step of 2% by changing the initial strain set to 28%, 30%, 32% and 34%. In the third set a strain step of 5% was used and the initial strain set included 25%, 30%, 35% and 40%. To demonstrate the validity of the procedure, an error parameter, error_l^{mn} is introduced in the form

$$\mathrm{error}_l^{mn}(\eta) = \left(\frac{\mathrm{d}F_l^{mn}(\eta)}{\mathrm{d}\eta}\Big|_{\mathrm{d}\eta=0.001}\right)_{\mathrm{cal}} - \left(\frac{\mathrm{d}F_l^{mn}(\eta)}{\mathrm{d}\eta}\Big|_{\mathrm{d}\eta=0.001}\right)_{\mathrm{Taylor}} \tag{8}$$

Fig. 2 shows a plot of error_l^{mn} as a function of strain for three different initial strain sets. It is clear that the errors of the rate of change of F_4^{11} from the simulation are low when the strain is taken as 20%. Since a strain of 30% is included in the initial set for the fitting, the corresponding error is zero. The error is maintained at a reasonably low value for a strain of 40% while it is dramatically increased for a strain of 50%. The same trend is reflected in Fig. 2(b) which illustrates the errors in the rate of change of F_4^{12}. When the strain step is within 1% or 2%, the simulation produces a large error (>0.2) when compared to Taylor's model at a strain of 20%. When the strain is within 30% or 40%, the error is within an acceptable range of 0.01 (except at a strain step of 1%). But with the increase of strain, the error increases to an unacceptable range, larger than 0.10 at a strain of 50%. Fig. 2(c) shows the variation of the error parameter for $\mathrm{d}F_4^{13}/\mathrm{d}\eta$. The error is smaller than 0.06 in the range of strains from 20% to 40% for all the three strain steps. When the strain is increased to 50%, the error is increased slightly to 0.08 (for a strain step of 5%), −0.39 (for a strain step of 2%) and 0.38 (for a strain step of 1%), respectively. Overall, we can see that the simulation is very close to Taylor's model in the strain range of 20–40%. It deviates from the prediction of Taylor's model when the strain is far from the initial strain set. It is clear from the results above that the procedure introduced in this

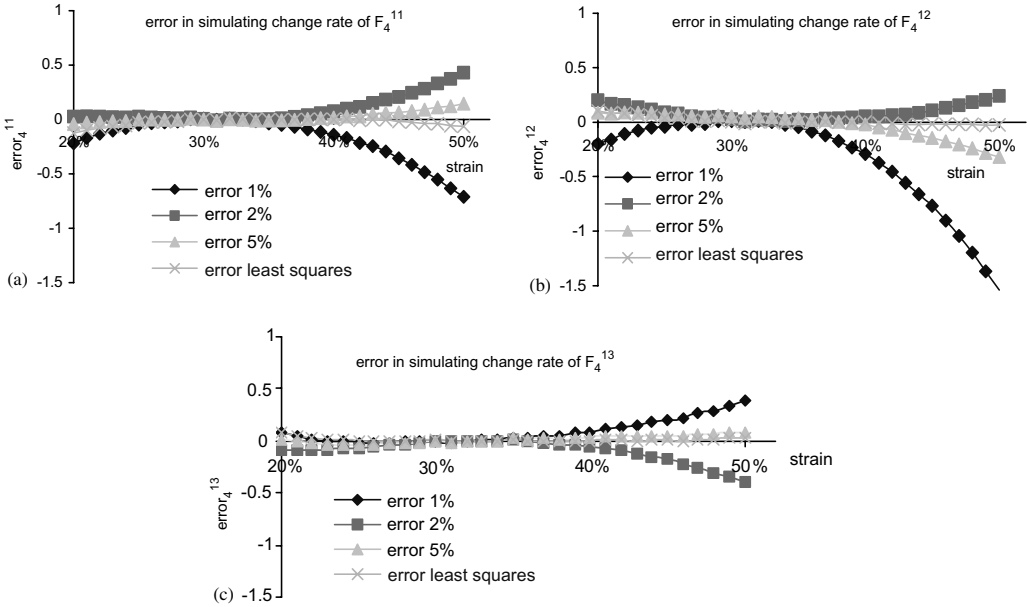

Fig. 2. (a) error_4^{11}, (b) error_4^{12}, (c) error_4^{13} as a function of strain when the simulation results are obtained using strain step as 1%, 2% and 5%, respectively. The error of simulation obtained from least squares method is also illustrated.

paper provides the best results when used for interpolation. This means that if the texture coefficients are predicted at a strain which is within the range of initial strain set, the error is minimum. If this prediction is extended to strains out of the range of the initial strain set, the farther the strain is from the range of the initial strain set, the worse the prediction of the texture evolution is. To compare the errors from different strain ranges, we define mean error $\overline{\text{error}}_l^{mn}$:

$$\overline{\text{error}}_l^{mn} = \frac{1}{N}\sum \text{error}_l^{mn} \tag{9}$$

Fig. 3 illustrates the mean error parameter for the three nonzero texture coefficients obtained from different strain steps. In the strain range from 20% to 50%, the simulation from strain step of 5% fits best to the Taylor's model. The simulation from strain step of 2% follows next. If the strain step is as small as 1%, the simulation in the large strain range will result in a large error. The mean error of the evolution rate parameter F_4^{12} is larger than the other two texture coefficients. Fig. 4 shows the evolution of these three texture coefficients during deformation process obtained from Taylor's model. Note that the magnitude of F_4^{12} is small compared to the other two, which results in larger variations in the error.

One of the contributions to the error is truncation error from Eq. (3). This linear approach works well in the deformation history close to the initial strain set. The $A_{\lambda l}^{\sigma\rho mn}$ obtained from the initial strain set does not predict the texture coefficients when the strain is far from the initial strain set. To overcome this limitation, different $A_{\lambda l}^{\sigma\rho mn}$

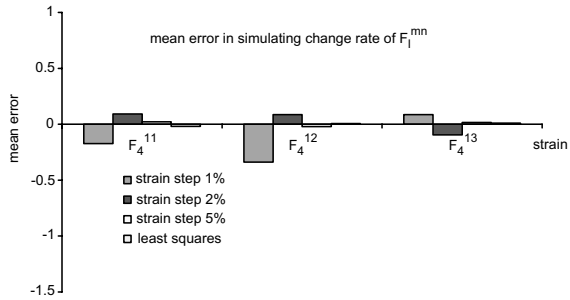

Fig. 3. $\overline{\text{error}}_l^{mn}$, mean error of texture evolution rate of F_4^{11}, F_4^{12} and F_4^{13} when the simulated results are obtained using different methods.

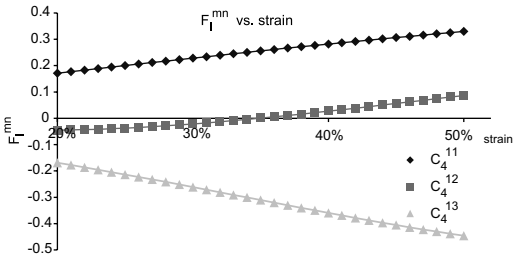

Fig. 4. Evolution of texture coefficients F_l^{mn} during deformation process using Taylor's model.

may be used in different deformation stages. For the deformation up to 100%, five matrices form of $A_{\lambda l}^{\sigma\rho mn}$ combined can be used to describe the processing path each covering a strain range of 20%. This approach is still a simple and efficient way in describing the processing path and streamlines for the deformation processes for a relatively large strain range.

Another approach to obtain the texture evolution coefficient is to use least squares estimates method. From $M+1$ texture data ($M > N$) at different strains, the texture evolution coefficient matrix A is calculated from the over-determined system below:

$$\lfloor \mathrm{d}F_l^{mn}(\eta)/\mathrm{d}\eta \rfloor = [A][F_l^{mn}(\eta)] \tag{10}$$

$\mathrm{d}F_l^{mn}(\eta)/\mathrm{d}\eta$ is an $N \times M$ matrix. $M+1$ is the dimension of the initial strain set. N is the number of texture coefficients we are interested in. A is an $N \times N$ matrix and $F_l^{mn}(\eta)$ is an $N \times M$ matrix.

Here we choose M as 10, the initial strain set from 30% to 41%, and the strain step as 1%. From the texture data at these strains, $A_{\lambda l}^{\sigma\rho mn}$ is calculated by least square fitting method. Using the resultant $A_{\lambda l}^{\sigma\rho mn}$, we simulate the evolution rate of texture coefficients during the deformation from 20% to 50%. The result is also shown in Fig. 2. To demonstrate the advantage of this method, the result of least squares method is compared with those from other three methods discussed before. Fig. 2 shows clearly that the $A_{\lambda l}^{\sigma\rho mn}$ obtained from linear solution at strain step of 1% or 2% does not describe the behavior as well as the $A_{\lambda l}^{\sigma\rho mn}$ obtained from the least squares method. The comparison of the least squares method with the linear method using a strain step of 5% is a little complicated. The latter one has a larger initial strain set range, from 20% to 40%, while the first one has a relatively smaller initial strain set range, from 30% to 40%. The fit for least squares method is not as good as the linear fit in the low strain range of around 20%, which is included in the initial strain set for the latter one but not in the initial strain set for the least squares method. The mean error in the strain range from 20% to 50% of the least squares method is still lower than that of the latter one. It is shown in the mean error illustrated in Fig. 3. Using least squares method we may obtain the texture evolution coefficients which can better describe the texture evolution behavior during mechanical deformation.

Acknowledgements

This work has been funded under the AFOSR grant # F49620-03-1-0011 and Army Research Lab contract # DAAD17-02-P-0398 and DAAD 19-01-1-0742.

References

[1] Bunge HJ. Z Metallkde 1965;56:872.
[2] Adams BL, Henrie A, Henrie B, Lyon M, Kalidindi SR, Garmestani H. J Mech Phys 2001;49:1639.
[3] Clement A. Mater Sci Eng 1982;55:203.
[4] Clement A, Coulomb P. Scripta Mater 1979;13:899.
[5] Bunge HJ, Esling C. Scripta Mater 1984;18:191.
[6] Kalidindi SR, Bronkhorst CA, Anand L. J Mech Phys 1992;40:537.
[7] Garmestani H, Kalidindi SR, Williams L, Baclatchuk CM, Fountain C, Lee EM, Se-Said OS. Int J Plast 2002;18:1373.
[8] Bunge HJ. Texture analysis in materials science: mathematical methods. London: Butterworth & Co; 1982. p. 340.